Transverse free vibration of non uniform rotating Timoshenko beams with elastically clamped boundary conditions

D. V. Bambill, C. A. Rossit, R. E. Rossi, D. H. Felix & A. R. Ratazzi

Meccanica
An International Journal of Theoretical and Applied Mechanics AIMETA

ISSN 0025-6455

Meccanica
DOI 10.1007/s11012-012-9668-5

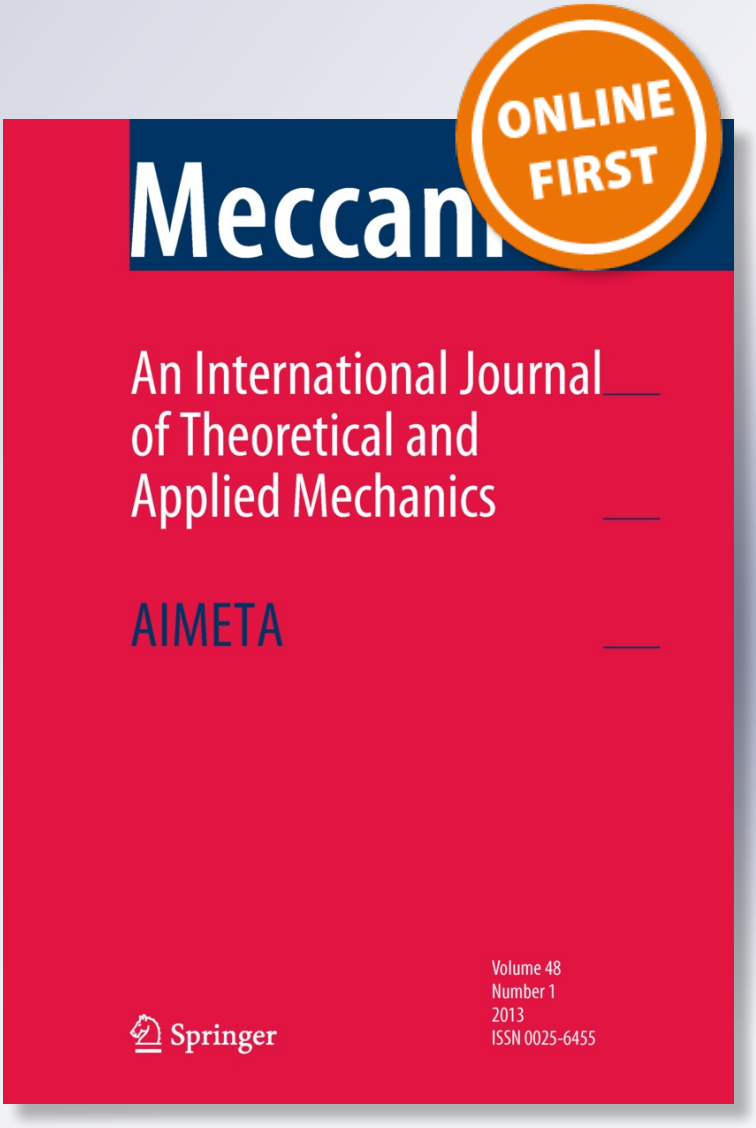

Springer

Meccanica
DOI 10.1007/s11012-012-9668-5

Transverse free vibration of non uniform rotating Timoshenko beams with elastically clamped boundary conditions

D.V. Bambill · C.A. Rossit · R.E. Rossi · D.H. Felix · A.R. Ratazzi

Received: 5 July 2012 / Accepted: 17 November 2012

Abstract In the present paper the Differential Quadrature Method, DQM, and the domain decomposition are used to carry out the free transverse vibration analysis of non-uniform multi-span rotating Timoshenko beams with perfect and not perfect boundary conditions. The cross section could vary in a continuous or discontinuous fashion along the beam length. The material of the beam could be different in each beam span. The influence of elastically clamped boundary conditions at hub end are studied and discussed. The effect of an arbitrary hub radius is considered. The governing differential equations of motion for rotating Timoshenko beams come from the derivation of Hamilton's principle. The first six natural frequencies of vibration are obtained for many particular situations and for some of them the mode shapes are also available. The examples of applications of the method indicated its effectiveness. The results for particular cases are in excellent agreement with published results and results obtained by means of the finite element method.

D.V. Bambill (✉) · C.A. Rossit · R.E. Rossi · D.H. Felix · A.R. Ratazzi
Instituto de Mecánica Aplicada, IMA, Departamento de Ingeniería, Universidad Nacional del Sur, UNS, Bahía Blanca, Argentina
e-mail: dbambill@criba.edu.ar

D.V. Bambill · C.A. Rossit
Consejo Nacional de Investigaciones Científicas y Técnicas, CONICET, Bahía Blanca, Argentina

Keywords Vibration · Rotating beams · Timoshenko · Tapered · Differential Quadrature Method · Elastic supports · Elastically clamped

1 Introduction

The dynamic behavior of rotating beams is of practical interest since it is widely used in many engineering applications. Rotating beams can be used to model steam and gas turbine blades, spinning space craft, helicopter rotor blades, gear teeth and the like.

The most simplified model, based on one dimensional Euler-Bernoulli theory, can be used for low natural frequencies of long slender beams, [1–7]. Hodges and Rutkowosky [1], used a variable order finite element method. Naguleswaran [2] described the lateral vibration of uniform beams with clamped, pinned and free boundary conditions, and expressed the general solution of the mode shape equation as the superposition of four linearly independent power series solution functions. In 2000 Banerjee [3] developed for the first time a dynamic stiffness matrix to study the free vibration characteristics of uniform and tapered rotating beams. Banerjee, Su and Jackson [4] presented a large range of examples of rotating beams, solved by the stiffness matrix method according to the Euler Bernoulli theory. They considered beams with linearly varying taper in depth and/or width of the cross section along the length that allows constructing different

Published online: 07 December 2012

cross sections which cover a large number of practical situations. Wang and Wereley [5] proposed a spectral finite element method to develop a low-degree-of-freedom model for dynamic analysis of rotating tapered Euler Bernoulli beams. Özdemir and Kaya [6] studied the out-of-plane free vibration analysis of a double tapered Euler–Bernoulli beam, mounted on the periphery of a rotating rigid hub, they used the differential transform method (DTM) to solve the governing differential equation of motion. Gunda and Ganguli [7] developed a new rotating beam finite element that satisfies the governing static homogeneous differential equations of Euler Bernoulli rotating beams. They successfully applied these elements to determined natural frequencies of uniform and tapered rotating beams with clamped and hinged boundary conditions.

As it is known Timoshenko theory of beams extended in the range of applicability the Euler Bernoulli theory, by taking into account effects of rotational inertia and transverse shear deformation. This extension leads to insignificant differences with the prediction of the Euler-Bernoulli model in the case of slender beams and low modes of vibration, but it can lead to important corrections in the case of short beams and when higher natural frequencies are determined.

Banerjee [8] in an outstanding work presented an important paper in which the corresponding governing differential equations of motion for rotating Timoshenko beams undergoing free natural vibrations were derived using Hamilton's principle and include the effect of an arbitrary hub radius. The relevance of a velocity dependent term was made clear and a free vibration analysis was carried out using the dynamics stiffness matrix, with the Frobenius method.

Özdemir and Kaya [9] used the differential transform method for free vibration analysis of a rotating tapered Timoshenko beam. Kumar and Ganguli [10] looked for rotating beams whose eigenpairs (frequency and mode shape) are the same as that of uniform not rotating beams for a particular mode. Ganesh and Ganguli [11] proposed a new physics based basis function for vibrating analysis of high speed rotating beams using the finite element method. The basis function gave rise to shape functions which depend on position of the element in the beam, material, geometric properties and rotational speed. Attarnejad and Shahba [12] introduced the concept of Basic Displacement Functions (BDFs) to study free vibrations of rotating tapered beams from a mechanical point of view and showed that exact shape functions could be derived in terms of BDFs. Allahverdizadeh et al. [13] analyzed the vibration properties of a rotating Functionally Graded Electro-Rheological beam using Hamilton's principle and finite element method.

The Differential Quadrature Method, DQM, has been successfully used to analyze vibration of beams. Laura and Gutiérrez [14] proposed in 1993, the analysis of vibrating Timoshenko beams using the DQM; and in 1996 Bert and Malik [15] presented a review of the DQM in computational mechanics. Karami and Malekzadeh [16] used the DQM for beam analysis and Karami, Malekzadeh and Shahpari [17] present the DQM as an alternative discrete approach for solving directly the governing equations for vibration of shear deformable non uniform beams. Liu and Wu [18] proposed a vibration analysis of Bernoulli beams using the differential quadrature rule and domain decomposition. More recently Felix et al. [19], and Bambill et al. [20, 21] used the differential quadrature method and the domain decomposition for determining natural frequencies and mode shapes of uniform and tapered rotating Timoshenko beams. Zong and Zhang [22], presented the latest important developments of Differential Quadrature methods in recent years.

The present paper deals with the transverse vibrations of cantilever rotating Timoshenko beams with many additional complexities. The equations of motion [8] are applied to multi-span beams with a variation of the mass per unit length. The beam model could have step jumps in its cross section or in the material properties, a tapered variation of the cross section, an elastic connection to the hub and an arbitrary hub radius. The natural frequencies and mode shapes for many numerical examples are obtained using the DQM and in some cases also with the finite element method. The authors present in this paper a continuation of their previous published work [19–21]; and analyze the effect of a non perfect clamped condition at the hub end on the frequencies and mode shapes of rotating beams. The effects of the radius of the hub and the slenderness ratio of the beam are analyzed too.

2 Theoretical considerations

The configuration of the structural beam system is illustrated in Fig. 1. The multi span beam of length L

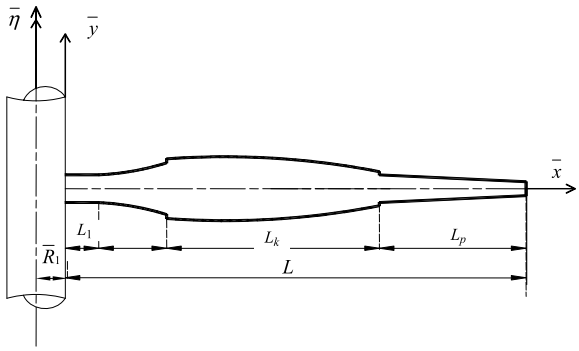

Fig. 1 Timoshenko rotating beam

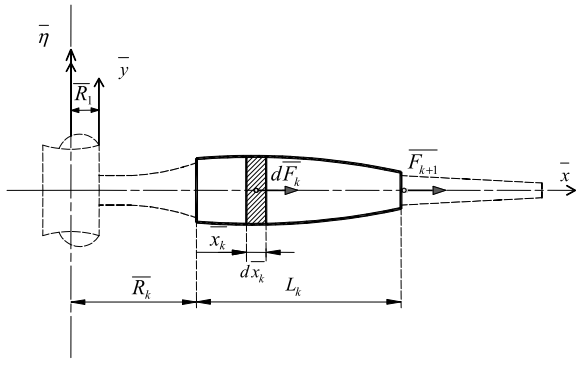

Fig. 2 Subdomain k of the Timoshenko rotating beam

is attached radially to the outside of a rotating hub with radius $\overline{R_1}$, that rotates at constant speed $\overline{\eta}$. The beam cross section is assumed to have doubly symmetry. The origin of the Cartesian coordinate system is at the hub end of the beam, the $\overline{x}$-axis coincides with the centroidal axis of the beam. The $\overline{y}$-axis is parallel to the axis of rotation and the $\overline{z}$-axis lies in the plane of rotation. A principal axis of the beam cross section is parallel to $\overline{y}$-axis. The hub is considered infinitely rigid in the $\overline{x}$-direction.

The mass $m(\overline{x})$ per unit length varies with the $\overline{x}$ coordinate. The edge attached to the hub is supposed elastically clamped. It may rotate around the $\overline{z}$-axis and translate in the $\overline{y}$-direction, while the elastic support reacts with a restoring moment proportional to the rotation angle and a restoring force proportional to the transversal displacement.

The beam domain is discretized into p subdomains depending on the geometric and/or material discontinuities. Figure 2 shows subdomain k.

The displacements $\overline{w}$ and rotation $\overline{\psi}$ in the $\overline{x}$–$\overline{y}$ plane due to bending and shear deformation are taken into account and the Coriolis effects are not considered. The boundary conditions at outer ends and the compatibility relations of internal forces and displacements between adjacent subdomains are included. The governing equations of motion were derived using Hamilton's principle [8].

Figure 2 shows the subdomain k of length L_k of the rotating beam.

The centrifugal force $d\bar{F}_k$, generated at a differential beam element located at $\overline{R}_k + \overline{x}_k$ is:

$$d\bar{F}_k = \bar{\eta}^2(\bar{R}_k + \bar{x}_k)\rho_k dV_k; \quad dV_k = A_k d\overline{x_k}; \tag{1}$$

with $A_k = A_k(\overline{x_k})$ the area of the cross section and ρ_k the mass density of the beam segment k at $\overline{x_k}$.

Then the internal tensile axial force $\bar{N}_k(\bar{x}_k)$ due to the rotational speed in the section of the beam at $(\overline{R}_k + \overline{x}_k)$, is:

$$\begin{aligned}\bar{N}_k &= \left(\int_{\bar{x}_k}^{L_k} d\bar{F}_k\right) + \overline{F}_{k+1};\\ \bar{N}_k(\bar{x}_k) &= \bar{\eta}^2\left(\bar{R}_k\int_{\bar{x}_k}^{L_k}\rho_k A_k(\bar{x}_k)\,d\bar{x}_k\right.\\ &\quad\left.+\int_{\bar{x}_k}^{L_k}\rho_k A_k(\bar{x}_k)\bar{x}_k\,d\bar{x}_k\right) + \overline{F}_{k+1},\end{aligned} \tag{2}$$

with $\overline{F}_{k+1}$ the outboard force at the end of the segment k, due to the adjacent segments from segment $k+1$ to the end segment p.

Assuming harmonic oscillation so that

$$\bar{w}_k(\bar{x}_k, t) = \bar{W}_k(\bar{x}_k)e^{i\omega t}; \tag{3a}$$

$$\bar{\psi}_k(\bar{x}_k, t) = \bar{\Psi}_k(\bar{x}_k)e^{i\omega t}; \tag{3b}$$

where ω is the circular frequency of oscillation in radians per second, and $\bar{W}_k$ and $\bar{\Psi}_k$ are the maximum amplitudes of the displacements $\bar{w}_k$ and $\bar{\psi}_k$.

The internal forces, shear force and bending moment at an instant t, in the section of the beam at $(\overline{R}_k + \overline{x}_k)$ from the axis of rotation are:

$$\bar{Q}_k^*(\bar{x}_k, t) = \bar{Q}_k(\bar{x}_k)e^{i\omega t}; \tag{4a}$$

$$\bar{M}_k^*(\bar{x}_k, t) = \bar{M}_k(\bar{x}_k)e^{i\omega t} \tag{4b}$$

with

$$\begin{aligned}\bar{Q}_k(\bar{x}_k) &= \left(\bar{N}_k(\bar{x}_k) + \kappa_k G_k A_k(\bar{x}_k)\right)\frac{d\bar{W}_k(\bar{x}_k)}{d\bar{x}_k}\\ &\quad - \kappa_k G_k A_k(\bar{x}_k)\bar{\Psi}_k(\bar{x}_k);\end{aligned} \tag{5}$$

$$\bar{M}_k(\bar{x}_k) = E_k I_k(\bar{x}_k)\frac{d\bar{\Psi}_k(\bar{x}_k)}{d\bar{x}_k} \tag{6}$$

$\bar{Q}_k(\bar{x}_k)$ and $\bar{M}_k(\bar{x}_k)$ are the maximum amplitudes of the shear force and the bending moment; with κ_k the shear factor; $G_k = E_k/2(1+\nu_k)$ the shear modulus, and ν_k the Poisson's ratio, and $I_k = I_k(\bar{x}_k)$ the second moment of area of the beam cross section and E_k the Young's modulus.

The governing differential equations of motion of a segment k of the rotating beam can be expressed as [8]:

$$-\frac{d\bar{Q}_k(\bar{x}_k)}{d\bar{x}_k} = \rho_k A_k(\bar{x}_k)\omega^2 \bar{W}_k(\bar{x}_k); \tag{7}$$

$$\begin{aligned}-\bar{Q}_k(\bar{x}_k) + \bar{N}_k(\bar{x}_k)\frac{d\bar{W}_k(\bar{x}_k)}{d\bar{x}_k} - \frac{d\bar{M}_k(\bar{x}_k)}{d\bar{x}_k} \\ - \rho_k I_k(\bar{x}_k)\bar{\eta}^2\bar{\Psi}_k(\bar{x}_k) = \rho_k I_k(\bar{x}_k)\omega^2\bar{\Psi}_k(\bar{x}_k)\end{aligned} \tag{8}$$

The term $\rho_k I_k(\bar{x}_k)\bar{\eta}^2\bar{\Psi}_k(\bar{x}_k)$ was introduced by Banerjee [8] and allows obtaining more realistic results, especially when the rotation speed is high.

Replacing Eqs. (5) and (6) into Eqs. (7) and (8), the equations of motion written in terms of the displacements and the centrifugal force are obtained:

$$\begin{aligned}&-\frac{d\bar{N}_k(\bar{x}_k)}{d\bar{x}_k}\frac{d\bar{W}_k(\bar{x}_k)}{d\bar{x}_k} - \bar{N}_k(\bar{x}_k)\frac{d^2\bar{W}_k(\bar{x}_k)}{d\bar{x}_k^2} \\ &\quad - \kappa_k G_k A_k(\bar{x}_k)\left(\frac{d^2\bar{W}_k(\bar{x}_k)}{d\bar{x}_k^2} - \frac{d\bar{\Psi}_k(\bar{x}_k)}{d\bar{x}}\right) \\ &\quad - \kappa_k G_k \frac{dA_k(\bar{x}_k)}{d\bar{x}_k}\left(\frac{d\bar{W}_k(\bar{x}_k)}{d\bar{x}_k} - \bar{\Psi}_k(\bar{x}_k)\right) \\ &\quad = \rho_k A_k(\bar{x}_k)\omega^2\bar{W}_k(\bar{x}_k)\end{aligned} \tag{9}$$

$$\begin{aligned}&-\kappa_k G_k A_k(\bar{x}_k)\left(\frac{d\bar{W}_k(\bar{x}_k)}{d\bar{x}_k} - \bar{\Psi}_k(\bar{x}_k)\right) \\ &\quad - E_k I_k(\bar{x}_k)\frac{d^2\bar{\Psi}_k(\bar{x}_k)}{d\bar{x}_k^2} \\ &\quad - E_k\frac{dI_k(\bar{x}_k)}{d\bar{x}_k}\frac{d\bar{\Psi}_k(\bar{x}_k)}{d\bar{x}_k} - \rho_k I_k(\bar{x}_k)\bar{\eta}^2\bar{\Psi}_k(\bar{x}_k) \\ &\quad = \rho_k I_k(\bar{x}_k)\omega^2\bar{\Psi}_k(\bar{x}_k)\end{aligned} \tag{10}$$

The compatibility conditions of internal forces and displacements between two adjacent beam segments k and $k+1$ are:

$$\bar{W}_k(L_k) - \bar{W}_{k+1}(0) = 0 \tag{11}$$

$$\bar{\Psi}_k(L_k) - \bar{\Psi}_{k+1}(0) = 0 \tag{12}$$

$$\bar{Q}_k(L_k) - \bar{Q}_{k+1}(0) = 0 \tag{13}$$

$$\overline{M_k}(L_k) - \overline{M}_{k+1}(0) = 0 \tag{14}$$

The boundary conditions at outer ends are:

(a) at $\overline{x_1} = 0$ in subdomain $k = 1$;

$$\bar{Q}_1(0) - \overline{K}_{W1}\bar{W}_1(0) = 0 \tag{15}$$

$$\bar{M}_1(0) - \overline{K}_{\Psi 1}\bar{\Psi}_1(0) = 0 \tag{16}$$

(b) at $\overline{x_p} = L_p$ in subdomain $k = p$;

$$\bar{Q}_p(L_p) = 0 \tag{17}$$

$$\bar{M}_p(L_p) = 0 \tag{18}$$

where $\bar{K}$ is used for the spring stiffness. For the elastic restrain against translation the subscript is W and for rotational spring the subscript is Ψ. Introducing a non-dimensional coordinate variable in each subdomain k:

$$x = \frac{\bar{x}_k}{L_k} \tag{19}$$

and taking dimensionless parameters as follows:

For lengths, distances and displacements:

$$\begin{aligned}&l_k = \frac{L_k}{L}; \qquad R_k = \frac{\overline{R}_k}{L}; \\ &W_k(x) = \frac{\bar{W}_k(\bar{x}_k)}{L_k}; \qquad \Psi_k(x) = \bar{\Psi}_k(\bar{x}_k).\end{aligned} \tag{20}$$

The spring constants parameters $\overline{K}$, are referred to the physical and geometrical characteristics of the beam:

$$\begin{aligned}&K_{Wi} = \overline{K}_{Wi}\frac{L}{E_1 A_1(0)}; \\ &K_{\Psi_i} = \overline{K}_{\Psi_i}\frac{L}{E_1 I_1(0)}, \quad \text{with } i = 1 \text{ and } i = p.\end{aligned} \tag{21}$$

The internal forces parameters are defined as:

$$\begin{aligned}&N_k(x) = \frac{\bar{N}_k(\bar{x}_k)}{E_k A_k(0)}; \qquad N_{k+1} = \frac{\overline{F}_{k+1}}{E_k A_k(0)}; \\ &Q_k(x) = \frac{\bar{Q}_k(\bar{x}_k)}{E_k A_k(0)}; \qquad M_k(x) = \frac{L_k}{E_k I_k(0)}\bar{M}_k(\bar{x}_k).\end{aligned}$$

The axial force expression (2) becomes

$$\begin{aligned}N_k(x) = \eta^2\frac{l_k^2}{s_1^2}\big(R_k v_k(1) + \phi_k(1) - R_k v_k(x) - \phi_k(x)\big) \\ + N_{k+1};\end{aligned} \tag{22}$$

where $s_k = L\sqrt{\frac{A_k(0)}{I_k(0)}}$ is the slenderness ratio, in particular s_1 is the slenderness ratio of the beam referred to the cross section closest to the hub: subdomain $k = 1$ at $x = 0$, and v_k and ϕ_k are:

$$v_k(x) = \frac{\int_0^x \rho_k A_k(x)dx}{l_k \rho_k A_k(0)};$$

$$\phi_k(x) = \frac{\int_0^x \rho_k A_k(x)x dx}{l_k^2 \rho_k A_k(0)}$$

The natural frequency and the rotational speed in their dimensionless form are expressed:

$$\Omega = \sqrt{\frac{\rho_1 A_1(0)}{E_1 I_1(0)}} L^2 \omega; \tag{23}$$

$$\eta^2 = \frac{\rho_1 A_1(0)}{E_1 I_1(0)} L^4 \bar{\eta}^2. \tag{24}$$

In the dimensionless form the governing differential equations (9) and (10) become:

$$\begin{aligned}
&\eta^2 a_k(x)(R_k + x)\frac{dW_k(x)}{dx} - \frac{s_1^2}{l_k^2} N_k(x)\frac{d^2 W_k(x)}{dx^2} \\
&\quad - \frac{\kappa_k}{2(1+\nu_k)}\frac{s_1^2}{l_k^2} a_k(x)\left(\frac{d^2 W_k(x)}{dx^2} - \frac{d\Psi_k(x)}{dx}\right) \\
&\quad - \frac{\kappa_k}{2(1+\nu_k)}\frac{s_1^2}{l_k^2}\frac{da_k(x)}{dx}\left(\frac{dW_k(x)}{dx} - \Psi_k(x)\right) \\
&\quad = \Omega^2 a_k(x) W_k(x);
\end{aligned} \tag{25}$$

$$\begin{aligned}
&- s_1^2 \frac{\kappa_k}{2(1+\nu)} s_k^2 a_k(x)\left(\frac{dW_k(x)}{dx} - \Psi_k(x)\right) \\
&\quad - \frac{s_1^2}{l_k^2} b_k(x)\frac{d^2\Psi_k(x)}{dx^2} \\
&\quad - \frac{s_1^2}{l_k^2}\frac{db_k(x)}{dx}\frac{d\Psi_k(x)}{dx} - \eta^2 b_k(x)\Psi_k(x) \\
&\quad = \Omega^2 b_k(x)\Psi_k(x);
\end{aligned} \tag{26}$$

where $a_k(x) = \rho_k A_k(x)/\rho_k A_k(0)$, and $b_k(x) = E_k I_k(x)/E_k I_k(0)$.

The compatibility conditions at adjacent subdomains k and $k+1$ expressed in terms of the dimensionless variables and parameters are:

$$l_k W_k(1) - l_{k+1} W_{k+1}(0) = 0 \tag{27}$$

$$\Psi_k(1) - \Psi_{k+1}(0) = 0 \tag{28}$$

$$\alpha_k Q_k(1) - \alpha_{k+1} Q_{k+1}(0) = 0; \tag{29}$$

$$\frac{\beta_k}{l_k} M_k(1) - \frac{\beta_{k+1}}{l_{k+1}} M_{k+1}(0) = 0; \tag{30}$$

where $\alpha_k = \rho_k A_k(0)/\rho_1 A_1(0)$, and $\beta_k = E_k I_k(0)/E_1 I_1(0)$.

And the boundary conditions at outer ends are:

(a) in subdomain $k = 1$, at $x = 0$:

$$Q_1(0) - K_{W1} l_1 W_1(0) = 0; \tag{31}$$

$$M_1(0) - K_{\Psi 1} l_1 \Psi_1(0) = 0; \tag{32}$$

(b) in subdomain $k = p$, at $x = 1$:

$$Q_p(1) = 0; \tag{33}$$

$$M_p(1) = 0. \tag{34}$$

3 The differential quadrature method

In order to obtain the DQM analog equations to the governing equations of the rotating beam and its continuity and boundary conditions [19, 21], the beam subdomains are discretized in a grid of n points using the Chebyshev–Gauss–Lobato expression [22]; in each subdomain k:

$$x_i = \frac{1 - \cos[(i-1)\pi/(n-1)]}{2}, \quad i = 1, 2, \ldots, n; \tag{35}$$

where x_i is the coordinate of node i. The q order derivatives of the displacements W and ψ, at a node i of the grid, based on the quadrature rules [15], are expressed:

$$\left.\frac{d^{(q)} W_k}{dx^q}\right|_{x_i} = \sum_{j=1}^{n} C_{ij}^{(q)} W_{kj}; \tag{36a}$$

$$\left.\frac{d^{(q)} \Psi_k}{dx^q}\right|_{x_i} = \sum_{j=1}^{n} C_{ij}^{(q)} \Psi_{kj} \tag{36b}$$

where W_{kj} and Ψ_{kj} are the displacements at node j of subdomain k, and the $C_{ij}^{(q)}$ are the weighting coefficients obtained using Lagrange interpolating functions [15, 17]:

$$\Pi(x_i) = \prod_{j=1\, j\neq 1}^{n} (x_i - x_j) \tag{37}$$

$$\begin{aligned}
C_{ij}^{(1)} &= \frac{\Pi(x_i)}{(x_i - x_j)\Pi(x_j)}, \quad q = 1; \\
C_{ij}^{(q)} &= C_{ii}^{(q-1)} C_{ij}^{(1)} - \frac{C_{ij}^{(q-1)}}{x_i - x_j}, \quad q > 1;
\end{aligned} \tag{38}$$

with $i, j = 1, 2, \ldots, n$, for $i \neq j$, and

$$\begin{aligned}
C_{ii}^{(1)} &= -\sum_{j=1\, j\neq i}^{n} C_{ij}^{(1)}, \quad q = 1; \\
C_{ii}^{(q)} &= -\sum_{j=1 \text{ with } j\neq i}^{n} C_{ij}^{(q)}, \quad q > 1;
\end{aligned} \tag{39}$$

$i, j = 1, 2, \ldots, n$, for $i = j$.

Using the quadrature rules, (36a), (36b), the differential quadrature analogs of the governing equations (25) and (26) of a node i are:

$$\left(\eta^2 a_k(x_i)(R_k+x_i) - \frac{\kappa_k}{2(1+\nu_k)}\frac{s_1^2}{l_k^2}\frac{da_k(x_i)}{dx}\right) \times \sum_{j=1}^{n}\left(C_{ij}^{(1)}\right)W_{kj} - \left(\frac{s_1^2}{l_k^2}N_k(x_i) + \frac{\kappa_k}{2(1+\nu_k)}\frac{s_1^2}{l_k^2}a_k(x_i)\right) \times \sum_{j=1}^{n}\left(C_{ij}^{(2)}\right)W_{kj} + \frac{\kappa_k}{2(1+\nu_k)}\frac{s_1^2}{l_k^2}a_k(x_i) \times \sum_{j=1}^{n}C_{ij}^{(1)}\Psi_{kj} + \frac{\kappa_k}{2(1+\nu_k)}\frac{s_1^2}{l_k^2}\frac{da_k(x_i)}{dx}\Psi_{ki} = \Omega^2 a_k(x_i)W_{ki} \tag{40}$$

$$-\frac{s_1^2 s_k^2\kappa_k}{2(1+\nu_k)}a_k(x_i)\sum_{j=1}^{n}C_{ij}^{(1)}W_{kj} - \frac{s_1^2}{l_k^2}b_k(x_i)\sum_{j=1}^{n}C_{ij}^{(2)}\Psi_{kj} + \left(\frac{s_1^2 s_k^2\kappa_k}{2(1+\nu_k)}a_k(x_i) - \eta^2 b_k(x_i)\right)\Psi_{ki} - \frac{s_1^2}{l_k^2}\frac{db_k(x_i)}{dx}\sum_{j=1}^{n}C_{ij}^{(1)}\Psi_{kj} = \Omega^2 b_k(x_i)\Psi_{ki} \tag{41}$$

The continuity equations (27) to (30) become:

$$l_k W_{kn} - l_{k+1}W_{(k+1)1} = 0; \tag{42}$$

$$\Psi_{kn} - \Psi_{(k+1)1} = 0; \tag{43}$$

$$\alpha_k\left(\left(N_k(1) + \frac{\kappa_k}{2(1+\nu_k)}a_k(1)\right) \times \sum_{j=1}^{n}C_{nj}^{(1)}W_{kj} - \frac{\kappa_k}{2(1+\nu_k)}a_k(1)\Psi_{kn}\right) - \alpha_{k+1}\left(\left(N_{k+1}(0) + \frac{\kappa_k}{2(1+\nu_k)}a_{k+1}(0)\right) \times \sum_{j=1}^{n}C_{1j}^{(1)}W_{(k+1)j} - \frac{\kappa_k}{2(1+\nu_k)}a_{k+1}(0)\Psi_{k1}\right) = 0; \tag{44}$$

$$\frac{\beta_k}{l_k}b_k(1)\sum_{j=1}^{n}C_{nj}^{(1)}\Psi_{kj} - \frac{\beta_{k+1}}{l_{k+1}}b_{k+1}(0)\sum_{j=1}^{n}C_{1j}^{(1)}\Psi_{(k+1)j} = 0; \tag{45}$$

and the boundary conditions (31)–(34):

$$\left(N_1(0) + \frac{\kappa_k}{2(1+\nu_k)}a_1(0)\right)\sum_{j=1}^{n}C_{1j}^{(1)}W_{1j} - \frac{\kappa_k}{2(1+\nu_k)}a_1(0)\Psi_{11} - l_1 K_{W1}W_{11} = 0; \tag{46}$$

$$K_{\Psi 1}\Psi_{11} - \frac{b_1(0)}{l_1}\sum_{j=1}^{n}C_{1j}^{(1)}\Psi_{1j} = 0; \tag{47}$$

$$\left(N_p(1) + \frac{\kappa_k}{2(1+\nu_k)}a_p(1)\right)\sum_{j=1}^{n}C_{nj}^{(1)}W_{pj} - \frac{\kappa_k}{2(1+\nu_k)}a_p(1)\Psi_{pn} = 0; \tag{48}$$

$$\frac{b_p(1)}{l_p}\sum_{j=1}^{n}C_{nj}^{(1)}\Psi_{pj} = 0. \tag{49}$$

The set of analog equations derived of the governing equations, the compatibility conditions between subdomains and the outer boundary conditions, is the linear system of equation that allows to determine the natural frequencies and the mode shapes of the rotating Timoshenko beam.

4 Numerical results

The convergence and accuracy of the present approach have been shown in previous papers, for uniform beams [20] and for non uniform Timoshenko beams with elliptical cross section [21]. In the present paper the rate of convergence and accuracy is demonstrated in Tables 1, 2 and 3.

The differential quadrature method is now been used to obtain the natural frequencies and mode shapes for rotating beams, which cross section varies in a continuous or discontinuous fashion along the beam length. The presence and dimension of the hub could be considered by varying the hub radius as a relation of the total length of the beam, and the boundary elastic conditions are varied to produce different situations.

Table 1 shows the convergence analysis for both methods.

Table 1 Convergence analysis: two span C-F beam, $\kappa = 0.849673$; $\nu = 0.30$; $R_1 = 0$; $s_1 = 30$; $l_1 = 2/3$; $\alpha_1 = 1$; $a_1(x) = 1+4x-2x^2$; $l_2 = 1/3$; $\alpha_2 = 3$; $a_2(x) = 1 - 0.9667x^2$

Method	n	Ω_1	Ω_2	Ω_3	Ω_4	Ω_5	Ω_6
		$\eta = 0$					
DQM	21	4.61575	38.9934	97.0540	152.849	206.827	210.234
	31	4.61574	38.9931	97.0534	152.848	206.827	210.234
	41	4.61573	38.9930	97.0532	152.848	206.827	210.235
	51	4.61573	38.9930	97.0532	152.848	206.827	210.235
		$\eta = 10$					
	21	10.9409	46.1049	106.420	164.422	207.532	224.087
	31	10.9409	46.1046	106.420	164.421	207.533	224.086
	41	10.9409	46.1045	106.420	164.421	207.534	224.086
	51	10.9409	46.1045	106.420	164.421	207.534	224.086
		$\eta = 15$					
	21	15.5212	53.2890	116.220	176.388	208.200	238.987
	31	15.5212	53.2887	116.219	176.387	208.201	238.986
	41	15.5212	53.2885	116.219	176.387	208.202	238.986
	51	15.5212	53.2885	116.219	176.387	208.202	238.986
	n_f	Ω_1	Ω_2	Ω_3	Ω_4	Ω_5	Ω_6
		$\eta = 0$					
FEM	300	4.61638	38.9941	97.0539	152.850	206.834	210.238
	750	4.61584	38.9932	97.0533	152.848	206.828	210.236
	1500	4.61576	38.9930	97.0532	152.848	206.828	210.235
	2000	4.61574	38.9930	97.0532	152.848	206.827	210.235
	3000	4.61574	38.9930	97.0532	152.848	206.827	210.235
		$\eta = 10$					
	300	11.0576	46.2437	106.476	164.464	207.743	224.114
	750	11.0573	46.2431	106.476	164.464	207.738	224.112
	1500	11.0573	46.2430	106.476	164.464	207.737	224.112
	2000	11.0572	46.2430	106.476	164.464	207.737	224.112
	3000	11.0572	46.2430	106.476	164.464	207.737	224.112
		$\eta = 15$					
	300	15.7014	53.5774	116.340	176.497	208.647	239.049
	750	15.7011	53.5771	116.340	176.497	208.642	239.048
	1500	15.7011	53.5770	116.340	176.497	208.642	239.048
	2000	15.7011	53.5770	116.340	176.497	208.642	239.048
	3000	15.7011	53.5770	116.340	176.497	208.642	239.048

Table 2 The first six natural frequency coefficients of a one span tapered cantilever beam, $\nu = 0.30$; $s_1 = 12.5$; $l_1 = 1$; $p = 1$; $\kappa = 0.849673$; $c_{01} = 1$; $c_{11} = -0.5$; $c_{21} = 0$

	η							
	0		3		5		10	
	DQM	[9]	DQM	[9]	DQM	[9]	DQM	[9]
Ω_1	3.64994	3.64996	4.88651	4.88654	6.47109	6.47110	10.9904	10.9905
Ω_2	15.0214	15.0218	16.4595	16.4599	18.7431	18.7434	26.9278	26.9280
Ω_3	32.7827	32.7840	34.4551	34.4564	37.2214	37.2226	47.8819	47.8827
Ω_4	53.3364	53.3391	55.3529	55.3555	58.7257	58.7281	71.9831	71.9847
Ω_5	75.4912	75.4955	77.8760	77.8802	81.8796	81.8834	97.6420	97.6447
Ω_6	98.1835	98.1897	100.913	100.919	105.459	105.464	119.884	119.891

The variations of the mass per unit length $m(x)$, as the beam is discretized in p subdomains, for each subdomain or segment k of the beam, is expressed as:

$$m_k(x) = \rho_k A_k(x) \tag{50}$$

The bending rigidity for the beam is:

$$E_k I_k(x) = \int_{m_k(x)} E_k y^2 \, dm_k \tag{51}$$

where y^2 is the square of the distance to the neutral bending axis of the cross section of the beam.

The beam cross section could vary at each subdomain in a quadratic fashion: the area is expressed as:

$$\begin{aligned} &A_k(x) = A_k(0) a_k(x); \\ &a_k(x) = c_{0k} + c_{1k} x + c_{2k} x^2 \end{aligned} \tag{52}$$

and the second moment of area:

$$\begin{aligned} &I_k(x) = I_k(0) b_k(x); \\ &b_k(x) = a_k(x)^3 = \left(c_{0k} + c_{1k} x + c_{2k} x^2\right)^3 \end{aligned} \tag{53}$$

where c_{0k}, c_{1k} and c_{2k} are constants.

The shear factor is evaluated for rectangular sections by the expression [23]:

$$\kappa = 10 \frac{(1+\nu)}{12 + 11\nu}; \tag{54}$$

with $\nu = 0.30$.

A convergence analysis is performed to select the number n of grid points in the DQM. The natural frequencies coefficients of a two span beam with unequal length subdomains are determined for the analysis. When the end of the beam tends to a small surface more grid points are necessary to achieve convergence. On account of this, $A_2(1)/A_1(0) = 0.1$ is adopted.

The finite element method, FEM, was used to obtain independent results of the natural frequencies coefficients of a cantilever Timoshenko rotating beam (C-F: clamped-free boundary conditions).

As it can be seen in Table 1, for the Differential Quadrature Method, $n = 41$ proved to be enough to capture accurately the dynamic behavior of the rotating beam.

On the other hand, the finite element model employed in the analysis, [24], has n_f beam elements of two nodes in the longitudinal direction. This beam model also takes into account the shear deformation (Timoshenko beam's theory), the rotational inertia and the increase in bending stiffness induced by the centrifugal force.

The FEM convergence analysis shows that taking $n_f > 2000$ in the formulation will not produce any improvement in the results.

The velocity dependent term, $\rho I_k(\bar{x}_k)\bar{\eta}^2 \bar{\Psi}_k(\bar{x}_k)$, of Eq. (10) is not included in the finite element formulation. Probably for that reason there are slight differences between the two sets of numerical results (DQM and FEM). As the rotational speed increases, the largest difference between the results of both methods, occur for the first frequency coefficient Ω_1: 1.05 % for $\eta = 10$ and 1.15 % for $\eta = 15$. For the second frequency coefficient Ω_2 the differences are reduced to 0.30 % for $\eta = 10$ and 0.54 % for $\eta = 15$, for the higher non-dimensional frequencies they are less than 0.10 %. The agreement is complete for the static case.

In Table 2 the first six non-dimensional frequencies obtained by DQM are compared with Özdemir and

Table 3 The first six natural frequency coefficients of a one span cantilever beam, C-F, with constant width and linearly varying thickness, when $A_1(1)$ approaches to zero. $\nu = 0.30$; $l_1 = 1$; $p = 1$; $\kappa = 0.849673$; $\eta = 12$

$A_1(1)/A_1(0)$	Ω_1	Ω_2	Ω_3	Ω_4	Ω_5	Ω_6	
	$s_1 = 1000$						
0.1	14.1227	30.7096	51.8090	79.5978	115.049	158.588	DQM
	14.1227	30.7096	51.8091	79.5978	115.049	158.588	FEM
0.01	14.4801	30.5480	49.0233	71.2795	98.0960	129.981	DQM
	14.4801	30.5482	49.0233	71.2795	98.0961	129.981	FEM
0.001	14.5280	30.6633	49.1654	71.2382	97.4444	128.102	DQM
	14.5281	30.6632	49.1655	71.2381	97.4443	128.102	FEM
0.0001	14.5331	30.6777	49.1973	71.2919	97.5203	128.190	DQM
	14.5331	30.6778	49.1972	71.2920	97.5200	128.189	FEM
0.00001	14.5336	30.6792	49.2007	71.2980	97.5303	128.204	DQM
	14.5335	30.6793	49.2006	71.2983	97.5300	128.204	FEM
0.000001	14.5336	30.6794	49.2010	71.2987	97.5311	128.206	DQM
	14.5336	30.6794	49.2010	71.2987	97.5312	128.206	FEM
	$s_1 = 30$						
0.1	13.9725	30.2037	50.2317	75.4683	105.957	141.181	DQM
	13.9833	30.2170	50.2486	75.4876	105.977	141.201	FEM
0.01	14.3213	30.0728	47.8006	68.5611	92.7265	120.347	DQM
	14.3327	30.0845	47.8137	68.5755	92.7415	120.362	FEM
0.001	14.3677	30.1813	47.9357	68.5546	92.2721	119.056	DQM
	14.3793	30.1930	47.9487	68.5686	92.2867	119.070	FEM
0.0001	14.3725	30.1950	47.9645	68.6024	92.3383	119.133	DQM
	14.3841	30.2067	47.9776	68.6164	92.3527	119.148	FEM
0.00001	14.3730	30.1964	47.9676	68.6078	92.3467	119.145	DQM
	14.3846	30.2081	47.9806	68.6219	92.3612	119.160	FEM
0.000001	14.3731	30.1965	47.9679	68.6084	92.3476	119.146	DQM
	14.3847	30.2082	47.9809	68.6224	92.3620	119.161	FEM

Kaya [9], the agreement between the results is very good (the biggest differences are less than 0.007 %).

A particular situation is presented in Table 3. As Banerjee has mentioned in [4], the present theory will cause numerical ill-conditioning when the beam end converge to a null cross section, therefore it can not be used when $A_p(1)/A_1(0) = 0$. The free vibration analysis of such a theoretical ended beam can be approximated taking $A_p(1)/A_1(0) \to 0$. The first frequency parameters increase as the area decreases; the other frequency parameters in general decrease. The DQM will need more than $n = 41$ points to extreme this condition, but the exact values will never be achieved because the theory does not take into account the condition of null area. The DQM results are obtained with $n = 91$ for $A_p(1)/A_1(0) = 0.000001$ and $n = 71$ for the other relations. The FEM results are obtained with $n_f = 3000$. Both methods provide the same accurate results for the slenderness ratio equal to 1000 and for the slenderness ratio equal to 30 again slight differences appeared. There is a difference of 0.08 % between the fundamental dimensionless frequencies, a difference of 0.04 % between the second dimension-

Table 4 The effect of the taper ratio and rotational speed on natural frequencies (lineal variation) one span C-F beam $l_1 = 1$; $s_1 \to \infty$; $\nu = 0.30$

$A_1(1)/A_1(0)$	9/10	7/10	1/2	3/10	1/10	
	$\eta = 0$					
Ω_1	3.55869	3.66674	3.82378	4.08170	4.63070	DQM
	3.55870	3.66675	3.82379	4.08171	4.63073	[4]
			3.8238			[5]
Ω_2	21.3380	19.8806	18.3172	16.6252	14.9308	DQM
	21.3381	19.8806	18.3173	16.6252	14.9308	[4]
			18.3173			[5]
Ω_3	58.9796	53.3219	47.2646	40.5875	32.8331	DQM
	58.9799	53.3222	47.2649	40.5879	32.8331	[4]
			47.2648			[5]
Ω_4	115.186	103.266	90.4496	76.1818	58.9168	DQM
Ω_5	190.143	169.858	147.999	123.542	93.3877	DQM
Ω_6	283.835	253.092	219.919	182.695	136.321	DQM
	$\eta = 5$					
Ω_1	6.49114	6.59525	6.74340	6.97847	7.44359	DQM
	6.49115	6.59525	6.74340	6.97848	7.44359	[4]
			6.74340			[5]
Ω_2	24.7804	23.3905	21.9052	20.3085	18.7412	DQM
	24.7805	23.3906	21.9053	20.3086	18.7412	[4]
			21.9053			[5]
Ω_3	62.5009	56.9108	50.9336	44.3802	36.8565	DQM
	62.5113	56.9112	50.9338	44.3805	36.8667	[4]
			50.9338			[5]
Ω_4	118.861	106.971	94.2055	80.0341	63.0139	DQM
Ω_5	193.908	173.637	151.812	127.431	97.5080	DQM
Ω_6	287.663	256.923	223.771	186.609	140.452	DQM
	$\eta = 10$					
Ω_1	11.2456	11.3524	11.5016	11.7315	12.1591	DQM
	11.2455	11.3523	11.5015	11.7314	12.1592	[4]
			11.5015			[5]
Ω_2	32.9968	31.6444	30.1826	28.5839	26.9695	DQM
	32.9968	31.6443	30.1827	28.5839	26.9695	[4]
			30.1827			[5]
Ω_3	71.9830	66.4500	60.5637	54.1457	46.8737	DQM
	71.9834	66.4503	60.5639	54.1459	46.8737	[4]
			60.5639			[5]
Ω_4	129.184	117.319	104.611	90.5723	73.9216	DQM
Ω_5	204.739	184.467	162.676	138.416	108.913	DQM
Ω_6	298.817	268.059	234.924	197.874	152.158	DQM

Table 5 Comparison of the non-dimensional natural frequencies of one span C-F uniform Timoshenko and Euler-Bernoulli beams. Rotational speed, $\eta = 0$ and 12; $l_1 = 1$; $\nu = 0.304$; $\kappa = 0.849673$

Beam theory	s_1	Ω_1	Ω_2	Ω_3	Ω_4	Ω_5	Ω_6	
	$\eta = 0$							
Timoshenko beam	30	3.479832	20.58883	53.33816	95.27369	143.1193	194.5319	DQM
		3.479832	*20.58883*	*53.33816*	*95.27371*	*143.1193*	*194.5320*	*FEM*
	60	3.506843	21.64309	59.19399	112.3402	178.7768	255.9961	DQM
		3.506842	*21.64309*	*59.19399*	*112.3402*	*178.7768*	*255.9961*	*FEM*
	1000	3.51598	22.0330	61.6875	120.867	199.767	298.354	DQM
		3.51598	*22.0330*	*61.6875*	*120.867*	*199.767*	*298.354*	*FEM*
	2000	3.51599	22.0341	61.6948	120.893	199.836	298.505	DQM
	4000	3.51599	22.0344	61.6966	120.900	199.854	298.543	DQM
	5000	3.51599	22.0344	61.6968	120.901	199.856	298.547	DQM
		3.51603	*22.0344*	*61.6968*	*120.901*	*199.856*	*298.547*	*FEM*
Euler Bernoulli beam		3.5160	22.0345	61.6972	–	–	–	[1]
		3.5160	22.0345	61.6972	120.902	199.860	–	[5]
		3.5160	22.0345	61.6972	120.902	199.862	–	[7]
	$\eta = 12$							
Timoshenko beam	30	12.9954	36.0022	71.7739	116.917	167.841	222.333	DQM
		13.0165	*36.0683*	*71.8362*	*116.970*	*167.886*	*222.371*	*FEM*
	60	13.1216	37.1526	77.1916	132.412	200.436	279.040	DQM
		13.1271	*37.1703*	*77.2102*	*132.430*	*200.453*	*279.055*	*FEM*
	1000	13.1700	37.6014	79.6050	140.501	220.447	319.708	DQM
		13.1700	*37.6015*	*79.6051*	*140.501*	*220.447*	*319.708*	*FEM*
	2000	13.1700	37.6027	79.6121	140.526	220.514	319.855	DQM
	4000	13.1701	37.6030	79.6139	140.532	220.531	319.892	DQM
	5000	13.1702	37.6031	79.6141	140.533	220.533	319.896	DQM
		13.1703	*37.6031*	*79.6141*	*140.533*	*220.533*	*319.896*	*FEM*
Euler Bernoulli beam		13.1702	37.6031	79.6145	–	–	–	[1]
		13.1702	37.6031	79.6146	140.534	220.536	–	[5]
		13.1702	37.6032	79.6146	140.533	220.539	–	[7]

less frequencies and smaller differences for the dimensionless higher frequencies (0.012 % or less for the sixth frequency coefficients).

The first six dimensionless natural frequencies for rotating beams of one span are obtained and compared with results from other authors (Table 4). The beam has cantilever boundary conditions and the cross section has constant width and linearly varying thickness, Eq. (52):

$$c_{01} = 1; \quad c_{11} = -0.1, -0.3, -0.5, -0.7, -0.9; \quad c_{21} = 0$$

The other dimensionless parameters are: $l_1 = 1$; $s_1 \to \infty$; $\kappa = 0.849673$; $\nu = 0.30$.

The same example has been studied by Banerjee [4], for the first three natural frequency coefficients. Wang et al. [5] presented only the case of $c_{11} = -0.5$. In the table it is possible to observe the effect of the taper ratio and rotational speed on the natural frequency

Table 6 The effect of the slenderness s_1 and the taper ratio on natural frequencies, rotational speed $\eta = 12$. Comparison with FEM (lineal variation) one span C-F beam ($l_1 = 1$) C-F

$A_1(1)/A_1(0)$	$\eta = 12$						
	1	9/10	7/10	1/2	3/10	1/10	
	$s_1 = 1000$						
Ω_1	13.1700	13.2135	13.3212	13.4710	13.7006	14.1227	DQM
	13.1700	13.2136	13.3212	13.4710	13.7006	14.1227	FEM
Ω_2	37.6014	36.9529	35.5827	34.0868	32.4269	30.7096	DQM
	37.6015	36.9530	35.5827	34.0868	32.4269	30.7096	FEM
Ω_3	79.6050	76.9394	71.4067	65.5194	59.0976	51.8090	DQM
	79.6051	76.9395	71.4068	65.5194	59.0976	51.8091	FEM
Ω_4	140.501	134.797	122.923	110.211	96.1819	79.5978	DQM
	140.501	134.797	122.923	110.211	96.1820	79.5978	FEM
Ω_5	220.447	210.726	190.451	168.662	144.428	115.049	DQM
	220.447	210.726	190.451	168.662	144.428	115.049	FEM
Ω_6	319.708	304.985	274.244	241.131	204.131	158.588	DQM
	319.708	304.985	274.244	241.131	204.131	158.588	FEM
	$s_1 = 60$						
Ω_1	13.1216	13.1668	13.2773	13.4296	13.6610	14.0832	DQM
	13.1271	13.1718	13.2814	13.4330	13.6640	14.0860	FEM
Ω_2	37.1526	36.5520	35.2677	33.8448	32.2452	30.5752	DQM
	37.1704	36.5677	35.2796	33.8532	32.2508	30.5789	FEM
Ω_3	77.1916	74.8245	69.8297	64.4019	58.3618	51.3804	DQM
	77.2102	74.8415	69.8436	64.4127	58.3695	51.3851	FEM
Ω_4	132.412	127.729	117.709	106.599	93.9170	78.4358	DQM
	132.430	127.745	117.723	106.610	93.9257	78.4415	FEM
Ω_5	200.436	193.197	177.487	159.707	138.900	112.379	DQM
	200.453	193.212	177.501	159.719	138.909	112.385	FEM
Ω_6	270.040	269.214	247.595	222.634	192.730	153.228	DQM
	279.055	269.229	247.608	222.645	192.739	153.235	FEM
	$s_1 = 30$						
Ω_1	12.9954	13.0439	13.1605	13.3178	13.5523	13.9725	DQM
	13.0165	13.0631	13.1763	13.3309	13.5636	13.9833	FEM
Ω_2	36.0022	35.5173	34.4432	33.2013	31.7532	30.2037	DQM
	36.0683	35.5756	34.4872	33.2326	31.7741	30.2170	FEM
Ω_3	71.7739	69.9870	66.0836	61.6432	56.4722	50.2317	DQM
	71.8362	70.0445	66.1311	61.6805	56.4991	50.2486	FEM
Ω_4	116.917	113.796	106.805	98.5621	88.5360	75.4683	DQM
	116.970	113.845	106.849	98.5987	88.5646	75.4876	FEM
Ω_5	167.841	163.593	153.856	141.978	126.918	105.957	DQM
	167.886	163.636	153.895	142.012	126.946	105.977	FEM
Ω_6	222.333	217.223	205.238	190.162	170.339	141.181	DQM
	222.371	217.259	205.272	190.192	170.365	141.201	FEM

Table 7 The effect of K_{W1} on the frequency parameters, with $K_{\psi 1} \to \infty$, for a two span-beam ($R_1 = 0$). $s_1 = 30$

K_{W1}	$\eta = 0$					
	Ω_1	Ω_2	Ω_3	Ω_4	Ω_5	Ω_6
$\to 0$	$\to 0$	8.93564	65.7124	123.119	180.171	207.223
0.01	1.87457	9.53329	65.8560	123.188	180.218	207.223
0.1	3.85522	14.1815	67.1295	123.807	180.642	207.224
0.5	4.44063	24.0769	72.2341	126.491	182.502	207.230
0.7	4.48946	26.5651	74.3997	127.771	183.410	207.233
1	4.52672	29.0866	77.1836	129.589	184.734	207.238
10	4.60667	37.6660	93.6046	147.284	201.985	207.429
100	4.61479	38.8569	96.6995	152.265	206.708	209.528
1000	4.61561	38.9793	97.0177	152.790	206.818	210.162
$\to \infty$	4.61573	38.9930	97.0532	152.848	206.827	210.235
	$\eta = 5$					
$\to 0$	$\to 0$	13.0595	68.4219	126.300	183.788	207.361
0.01	1.94350	13.4438	68.5538	126.364	183.833	207.361
0.1	4.80183	16.6999	69.7238	126.947	184.235	207.363
0.2	5.59355	19.6316	70.9824	127.589	184.680	207.364
0.5	6.25246	25.3810	74.4475	129.472	186.001	207.370
1	6.51123	30.3160	79.1289	132.398	188.123	207.380
10	6.76174	39.4485	95.8249	150.026	204.940	207.883
1000	6.79030	40.9169	99.5283	155.892	207.133	213.717
100000	6.79058	40.9321	99.5666	155.954	207.136	213.802
$\to \infty$	6.79061	40.9323	99.5671	155.954	207.136	213.803
	$\eta = 10$					
$\to 0$	$\to 0$	20.7259	75.4894	134.874	193.437	207.932
0.01	1.98196	20.9376	75.5963	134.929	193.476	207.932
0.1	5.62552	22.7904	76.5456	135.426	193.822	207.940
0.2	7.16489	24.6754	77.5716	135.975	194.205	207.949
0.5	8.94043	29.1078	80.4425	137.584	195.339	207.978
0.7	9.42517	31.2557	82.1726	138.620	196.079	207.999
1	9.83179	33.6790	84.4938	140.109	197.160	208.035
10	10.8196	44.1486	101.804	157.462	207.218	214.925
1000	10.9397	46.0839	106.371	164.345	207.532	223.980
100000	10.9409	46.1042	106.419	164.420	207.534	224.085
$\to \infty$	10.9409	46.1045	106.420	164.421	207.534	224.086
	$\eta = 15$					
$\to 0$	$\to 0$	28.9185	85.0476	146.951	203.803	212.183
0.01	1.99452	29.0502	85.1303	146.996	203.821	212.198
0.1	5.96190	30.2120	85.8667	147.401	203.979	212.339
0.2	7.95220	31.4407	86.6670	147.847	204.147	212.501
0.5	10.8111	34.6542	88.9439	149.159	204.610	213.019
0.7	11.7680	36.4138	90.3524	150.009	204.886	213.387
0.9	12.4074	37.9132	91.6717	150.837	205.135	213.773
1	12.6532	38.5790	92.2983	151.241	205.251	213.971
2	13.9272	43.1595	97.4656	154.928	206.128	216.073
10	15.1751	50.5430	110.177	167.955	207.684	227.863
10000	15.5209	53.2855	116.213	176.378	208.202	238.972
$\to \infty$	15.5212	53.2885	116.219	176.387	208.202	238.986

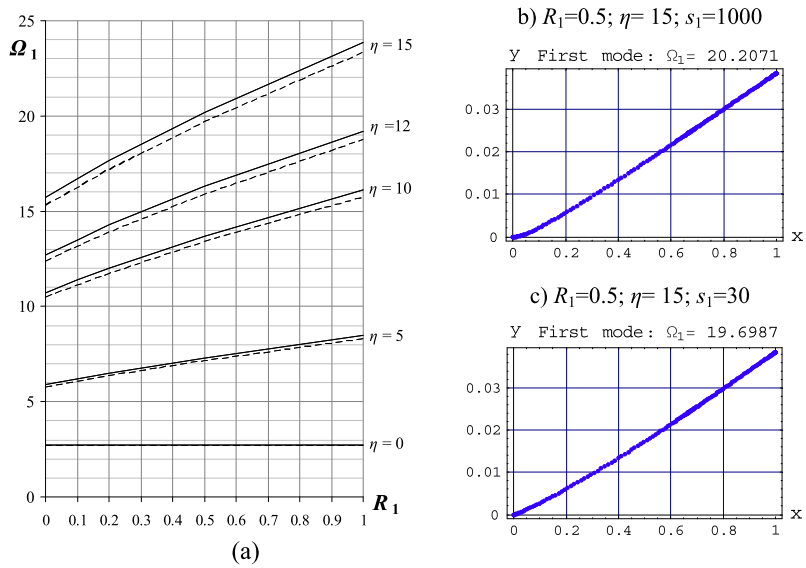

Fig. 3 (**a**) The effect of the hub ratio R_1 on the first natural frequency coefficients of a two span C-F beam with rotational speeds $\eta = 0, 5, 10, 15$. (- - - $s_1 = 30$; — $s_1 = 1000$.) (**b**) Mode shape for $R_1 = 0.5$; $\eta = 15$; $s_1 = 1000$. (**c**) Mode shape for $R_1 = 0.5$; $\eta = 15$; $s_1 = 30$

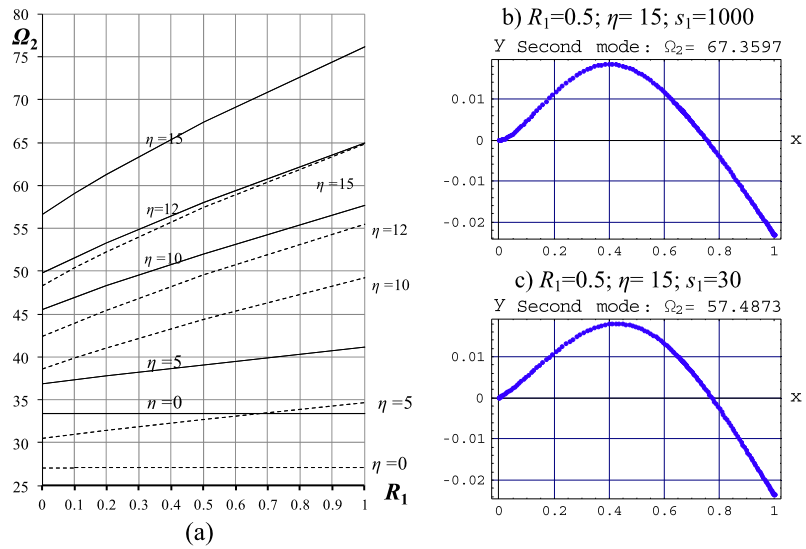

Fig. 4 (**a**) The effect of the hub ratio R_1 on the second natural frequency coefficients of a two span C-F beam with rotational speeds $\eta = 0, 5, 10, 15$. (- - - $s_1 = 30$; — $s_1 = 1000$.) (**b**) Mode shape for $R_1 = 0.5$; $\eta = 15$; $s_1 = 1000$. (**c**) Mode shape for $R_1 = 0.5$; $\eta = 15$; $s_1 = 30$

coefficients. The DQM coefficients are obtained with $n = 51$ grid points. The agreement between the three sets of results is excellent and proves the computation efficiency of the differential quadrature method.

Table 6 shows a comparison of the non-dimensional natural frequencies of one span C-F beam, for different slenderness ratios and rotating speed $\eta = 12$. In particular, the present results for large slenderness ra-

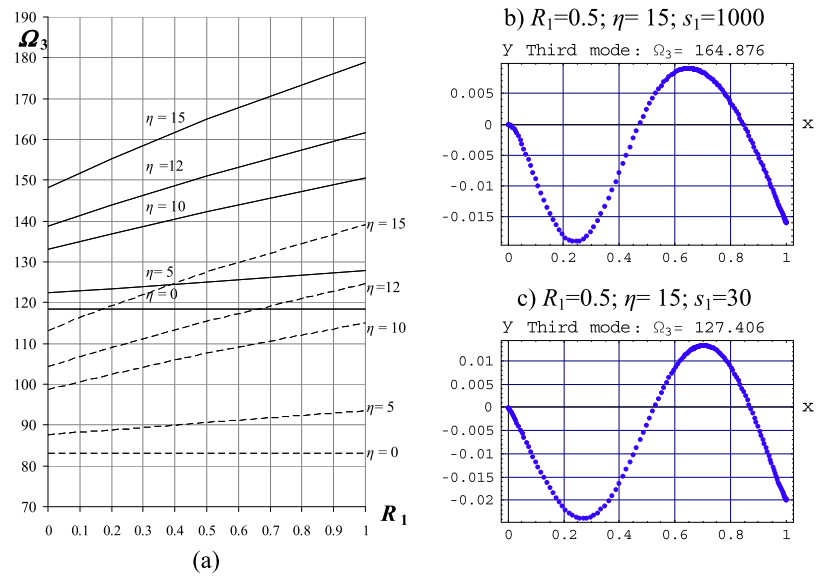

Fig. 5 (**a**) The effect of the hub ratio R_1 on the third natural frequency coefficients of a two span C-F beam with rotational speeds $\eta = 0, 5, 10, 15$. (- - - $s_1 = 30$; — $s_1 = 1000$.) (**b**) Mode shape for $R_1 = 0.5$; $\eta = 15$; $s_1 = 1000$. (**c**) Mode shape for $R_1 = 0.5$; $\eta = 15$; $s_1 = 30$

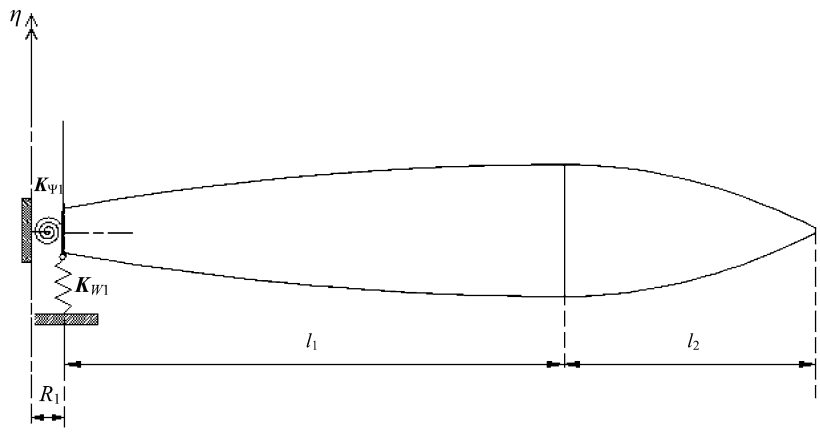

Fig. 6 Imperfect boundary condition at the hub of a two-span rotating beam

tios compare accurately with the Euler-Bernoulli results [1, 5, 7].

And again, small differences between DQM and FEM results appeared for lower slenderness ratios, for $s_1 = 30$: 0.16 % for Ω_1; 0.18 % for Ω_2; 0.09 % for Ω_3; and for $s_1 = 60$: 0.04 % for Ω_1; 0.05 % for Ω_2; 0.02 % for Ω_3.

In Table 6, the first six frequency coefficients are presented for three slenderness ratios, when the tapered beam rotates with $\eta = 12$.

The DQM and FEM results are in excellent agreement for the slenderness ratio equal to 1000, and again very small differences occur between both methods when the slenderness ratio is reduced. The largest difference between the values of both methods, is 0.18 %, and corresponds to the second non-dimensional frequency of the uniform beam with $s_1 = 30$.

Figures 3, 4 and 5 illustrate the effect of the hub ratio on the first three non-dimensional natural frequencies for beams with two different slenderness parame-

Table 8 The effect of K_{W1} on the frequency parameters, with $K_{\psi 1} \to \infty$, for a two span-beam ($R_1 = 1$). $s_1 = 30$

K_{W1}	$\eta = 5$					
	Ω_1	Ω_2	Ω_3	Ω_4	Ω_5	Ω_6
$\to 0$	$\to 0$	17.4173	72.4680	131.215	189.347	207.702
0.01	1.97207	17.6789	72.5831	131.274	189.388	207.702
0.1	5.38429	19.9604	73.6055	131.799	189.754	207.706
0.2	6.65538	22.2153	74.7087	132.377	190.160	207.709
0.5	7.94985	27.2031	77.7797	134.075	191.363	207.721
1	8.53256	31.9923	82.0522	136.733	193.300	207.742
10	9.13631	42.0465	99.1750	154.191	207.005	211.098
1000	9.20733	43.8020	103.411	160.696	207.456	219.501
100000	9.20805	43.8203	103.456	160.766	207.458	219.598
$\to \infty$	9.20808	43.8206	103.456	160.767	207.458	219.599
	$\eta = 10$					
$\to 0$	$\to 0$	30.0788	87.3268	150.081	205.054	215.020
0.01	1.99616	30.1969	87.4021	150.122	205.065	215.039
0.1	6.00805	31.2426	88.0729	150.493	205.169	215.212
0.2	8.06662	32.3598	88.8036	150.902	205.279	215.408
0.5	11.1213	35.3507	90.8946	152.107	205.585	216.011
0.7	12.1785	37.0354	92.1992	152.889	205.769	216.425
1	13.1749	39.1557	94.0186	154.027	206.018	217.059
10	16.1068	51.8230	112.065	170.375	208.098	230.897
1000	16.5133	54.9027	118.670	179.300	208.755	242.614
100000	16.5174	54.9363	118.744	179.404	208.762	242.763
$\to \infty$	16.5175	54.9364	118.744	179.404	208.763	242.763
	$\eta = 15$					
$\to 0$	$\to 0$	42.6956	104.674	173.036	206.936	241.879
0.01	2.00212	42.7642	104.724	173.064	206.940	241.898
0.1	6.18341	43.3755	105.178	173.320	206.972	242.071
0.2	8.52372	44.0403	105.675	173.603	207.008	242.263
0.5	12.5354	45.9281	107.123	174.438	207.114	242.836
0.7	14.1836	47.0894	108.050	174.983	207.185	243.214
1	15.9336	48.6820	109.383	175.781	207.291	243.775
2	19.0033	52.8423	113.312	178.266	207.638	245.584
10	22.9029	63.0544	127.452	189.411	209.903	255.750
10000	24.1572	68.3437	137.793	198.352	214.849	269.779
$\to \infty$	24.1585	68.3499	137.805	198.360	214.858	269.799

Table 9 The effect of $K_{\psi 1}$ on the frequency parameters, with $K_{W1} \to \infty$, for a two span-beam clamped at the rotational axis ($R_1 = 0$). $s_1 = 30$

$K_{\psi 1}$	$\eta = 0$					
	Ω_1	Ω_2	Ω_3	Ω_4	Ω_5	Ω_6
$\to 0$	$\to 0$	34.7237	92.9283	150.097	204.926	209.454
0.01	0.117491	34.7261	92.9302	150.099	204.927	209.454
0.1	0.370465	34.7469	92.9481	150.110	204.937	209.456
1	1.13908	34.9450	93.1186	150.220	205.026	209.475
10	2.89619	36.2343	94.2758	150.972	205.615	209.627
100	4.29728	38.3354	96.3512	152.364	206.556	210.040
1000	4.58068	38.9167	96.9704	152.791	206.797	210.210
10000	4.61219	38.9852	97.0447	152.842	206.824	210.232
100000	4.61538	38.9922	97.0523	152.848	206.827	210.235
$\to \infty$	4.61538	38.9922	97.0523	152.848	206.827	210.235
	$\eta = 5$					
$\to 0$	4.88918	37.1414	95.7624	153.411	205.899	212.481
0.01	4.89058	37.1434	95.7642	153.412	205.900	212.482
0.1	4.90307	37.1615	95.7806	153.423	205.906	212.487
1	5.01932	37.3332	95.9370	153.524	205.965	212.531
10	5.69025	38.4610	97.0000	154.221	206.349	212.855
100	6.55893	40.3357	98.9158	155.508	206.955	213.541
1000	6.76454	40.8629	99.4901	155.901	207.115	213.771
100000	6.79035	40.9316	99.5663	155.954	207.135	213.803
1000000	6.79058	40.9322	99.5670	155.954	207.136	213.803
$\to \infty$	6.79061	40.9323	99.5671	155.954	207.136	213.803
	$\eta = 10$					
$\to 0$	9.77617	43.2486	103.316	162.372	206.649	222.707
0.01	9.77686	43.2501	103.317	162.373	206.650	222.707
0.1	9.78302	43.2630	103.330	162.381	206.654	222.713
1	9.84123	43.3863	103.456	162.464	206.692	222.768
10	10.2090	44.2097	104.315	163.028	206.947	223.143
100	10.7724	45.6349	105.881	164.063	207.389	223.841
1000	10.9216	46.0494	106.356	164.378	207.517	224.057
10000	10.9390	46.0989	106.413	164.417	207.532	224.083
1000000	10.9409	46.1044	106.420	164.421	207.534	224.086
$\to \infty$	10.9409	46.1045	106.420	164.421	207.534	224.086
	$\eta = 15$					
$\to 0$	14.6601	51.2369	113.812	174.936	207.287	237.961
0.01	14.6605	51.2379	113.813	174.937	207.288	237.962
0.1	14.6646	51.2468	113.823	174.943	207.292	237.966
1	14.7033	51.3316	113.920	175.002	207.329	238.009
10	14.9577	51.9061	114.579	175.405	207.583	238.298
100	15.3842	52.9376	115.796	176.136	208.044	238.812
1000	15.5052	53.2470	116.169	176.358	208.183	238.965
10000	15.5196	53.2843	116.214	176.384	208.200	238.984
1000000	15.5211	53.2881	116.219	176.387	208.202	238.986
$\to \infty$	15.5212	53.2885	116.219	176.387	208.202	238.986

Table 10 The effect of $K_{\psi 1}$ on the frequency parameters, with $K_{W1} \to \infty$, for a two span-beam clamped at the rotational axis ($R_1 = 1$)

$K_{\psi 1}$	$\eta = 5$					
	Ω_1	Ω_2	Ω_3	Ω_4	Ω_5	Ω_6
$\to 0$	7.91942	40.6795	100.140	158.551	206.524	218.178
0.01	7.92022	40.6811	100.142	158.553	206.524	218.179
0.1	7.92740	40.6956	100.156	158.562	206.529	218.184
1	7.99498	40.8334	100.291	158.651	206.571	218.239
10	8.41366	41.7484	101.211	159.259	206.846	218.617
100	9.02939	43.3114	102.883	160.378	207.310	219.341
1000	9.18765	43.7610	103.388	160.721	207.441	219.568
100000	9.20787	43.8200	103.455	160.766	207.458	219.599
1000000	9.20805	43.8205	103.456	160.767	207.458	219.599
$\to \infty$	9.20808	43.8206	103.456	160.767	207.458	219.599
	$\eta = 10$					
$\to 0$	15.7993	53.1414	116.598	178.162	207.840	241.880
0.01	15.7996	53.1422	116.599	178.163	207.841	241.881
0.1	15.8029	53.1499	116.608	178.168	207.844	241.885
1	15.8342	53.2231	116.693	178.219	207.882	241.922
10	16.0425	53.7213	117.280	178.565	208.137	242.173
100	16.4001	54.6256	118.365	179.190	208.602	242.615
1000	16.5037	54.8996	118.699	179.379	208.743	242.745
10000	15.5196	53.2843	116.214	176.384	208.200	238.984
1000000	16.5174	54.9363	118.744	179.404	208.762	242.763
$\to \infty$	16.5175	54.9364	118.744	179.404	208.763	242.763
	$\eta = 15$					
$\to 0$	23.6573	67.2624	136.395	198.245	213.408	269.728
0.01	23.6576	67.2629	136.396	198.245	213.409	269.728
0.1	23.6597	67.2673	136.402	198.245	213.415	269.728
1	23.6799	67.3099	136.457	198.250	213.474	269.732
10	23.8177	67.6034	136.839	198.284	213.877	269.753
100	24.0707	68.1546	137.553	198.341	214.608	269.788
1000	24.1481	68.3265	137.775	198.358	214.829	269.797
10000	24.1575	68.3474	137.802	198.360	214.855	269.799
100000	24.1584	68.3496	137.805	198.360	214.858	269.799
$\to \infty$	24.1585	68.3499	137.805	198.360	214.858	269.799

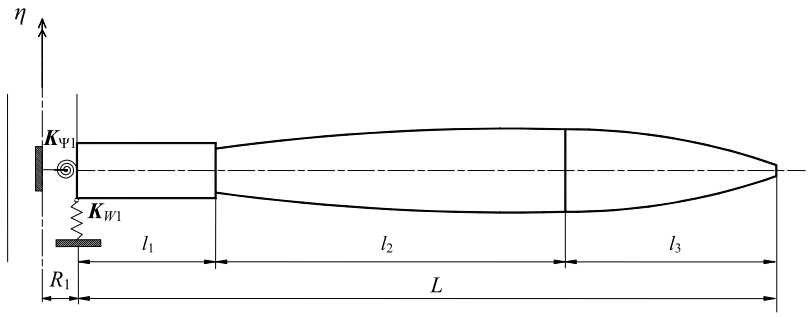

Fig. 7 Three span rotating Timoshenko beam with one step jump

ters $s_1 = 1000$ and $s_1 = 30$. The results correspond to a clamped-free beam with two spans. The cross section vary at each subdomain in a quadratic fashion: $l_1 = 2/3$, $\alpha_1 = 1$; $a_1(x) = 1 + 4x - 2x^2$, $l_2 = 1/3$, $\alpha_2 = 3$, $a_2(x) = 1 - 0.967x^2$. The frequency coefficients increase with the hub ratio as expected, because the centrifugal force increases with the distance to the axis of rotation and therefore also the stiffness of the beam.

The effect of the slenderness ratio, $s_1 = 1000$ and $s_1 = 30$, on the frequencies may be of considerable importance when studying the modes of vibration of higher frequencies, when a vibrating beam is subdivided by modal cross sections into comparatively short portions [25]. As it can be seen in Fig. 3, the effect of the slenderness ratio on the fundamental frequency is not significant as the first mode of vibration has only one nodal point.

For higher modes the effect of the cross sectional dimensions on the frequencies is more important. See Figs. 4 and 5 for second and third frequencies.

In the next example, Fig. 6, a beam with variable cross section is considered to study the effect of elastic supports on the frequency coefficients when the beam rotates. The beam has two spans and its characteristics are: $\nu = 0.30$; $\kappa = 0.849673$; $s_1 = 30$; for $k = 1$: $l_1 = 2/3$; $\alpha_1 = 1$; $c_{01} = 1$; $c_{11} = 4$; $c_{21} = -2$ and for $k = p = 2$: $l_2 = 1/3$; $\alpha_2 = 3$; $c_{02} = 1$; $c_{12} = 0$; $c_{22} = -0.9667$.

Tables 7, 9 and 10 present the situation in which the boundary condition at the hub is not a perfect clamped condition. In the y direction, the translational spring (K_{W1}) allows small displacements and the rotational spring ($K_{\psi 1}$) controls the rotation of the section closest to the hub.

The effect of the hub ratio is taken into account in Tables 8 and 10.

Table 7 provides numerical results for the spring constant K_{W1}, which varies between 0 and ∞, and the rotational spring constant is kept in $K_{\psi 1} \to \infty$.

The frequency coefficients for each rotational speed vary according to the boundary situation. The static situation, when $\eta = 0$, appears in the first part of the table.

It is observed that the fundamental frequency coefficients are the most affected in all cases. The condition $K_{W1} \to \infty$ is the condition of infinite stiffness, which leads to set up a perfectly clamped edge. Depending on the speed of rotation, K_{W1} values between 0 and 0.5 generate important changes in the lower no dimensional frequencies, for values of K_{W1} greater than one, the changes are quite minor and in general its influence disappears for values equal to 10 or more. The effect on the higher frequencies is not very significant.

Table 8 shows similar results considering a hub ratio R_1. The results showed the effects of the hub ratio and an imperfect boundary condition. Naturally, the hub ratio R_1 has no effect on the static situation, when $\eta = 0$, and this case is not repeated in the table.

Tables 9 and 10 show the effect of the rotational spring on the non-dimensional frequencies: for $K_{W1} \to \infty$ and values of $K_{\psi 1}$ from zero to infinity. The influence of this boundary condition is much less noticeable than the previous case. It can be said that the non-dimensional fundamental frequency is the most affected. However, as the rotational speed increases this effect tends to be less perceptible. For example, with $\eta = 15$, when $K_{\psi 1}$ varies from zero to infinity, the first frequency coefficient varies from 14.6601 to 15.5212 (5.5 %) and the sixth frequency

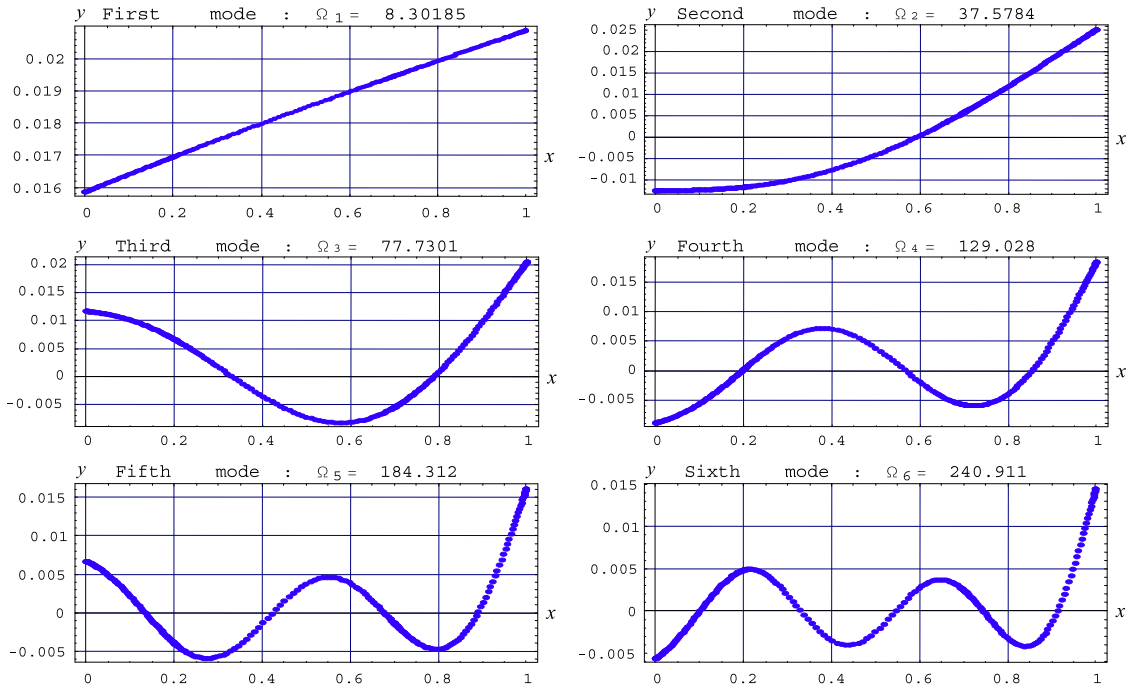

Fig. 8 The non-dimensional natural frequencies and mode shapes of a three span Timoshenko beam $R_1 = 0.5$; $s_1 = 30$; $K_{W1} = 0.1$; $K_{\psi 1} = 0.01$, $\eta = 15$

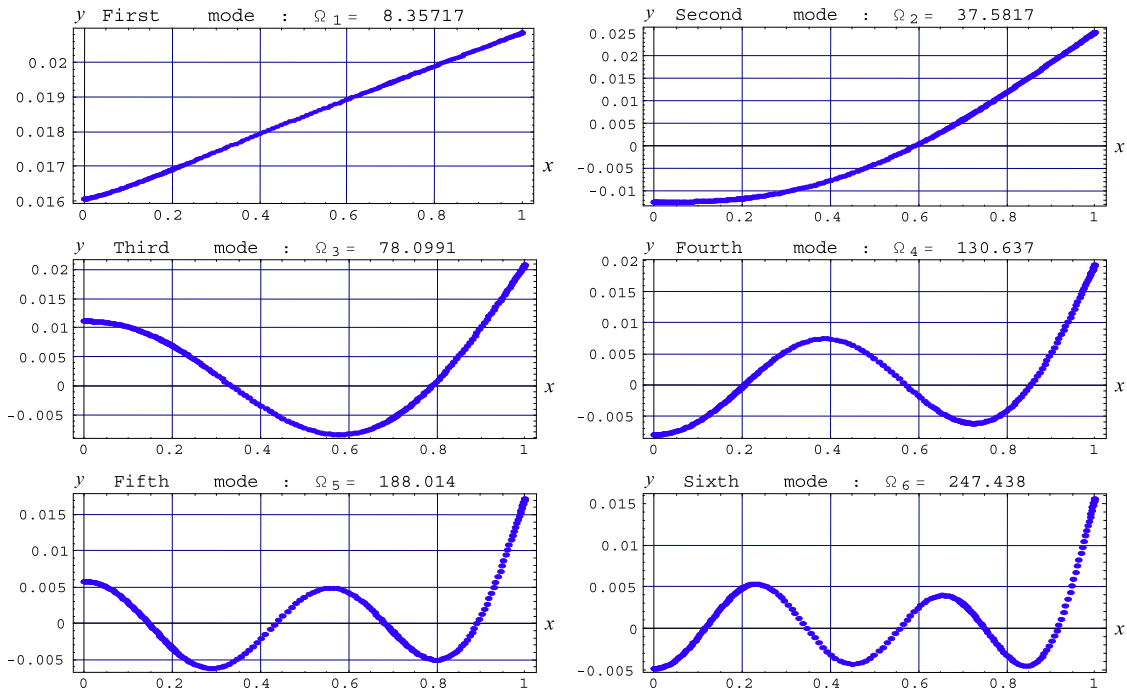

Fig. 9 The non-dimensional natural frequencies and mode shapes of a three span Timoshenko beam $R_1 = 0.5$; $s_1 = 30$; $K_{W1} = 0.1$; $K_{\psi 1} = 1000000$, $\eta = 15$

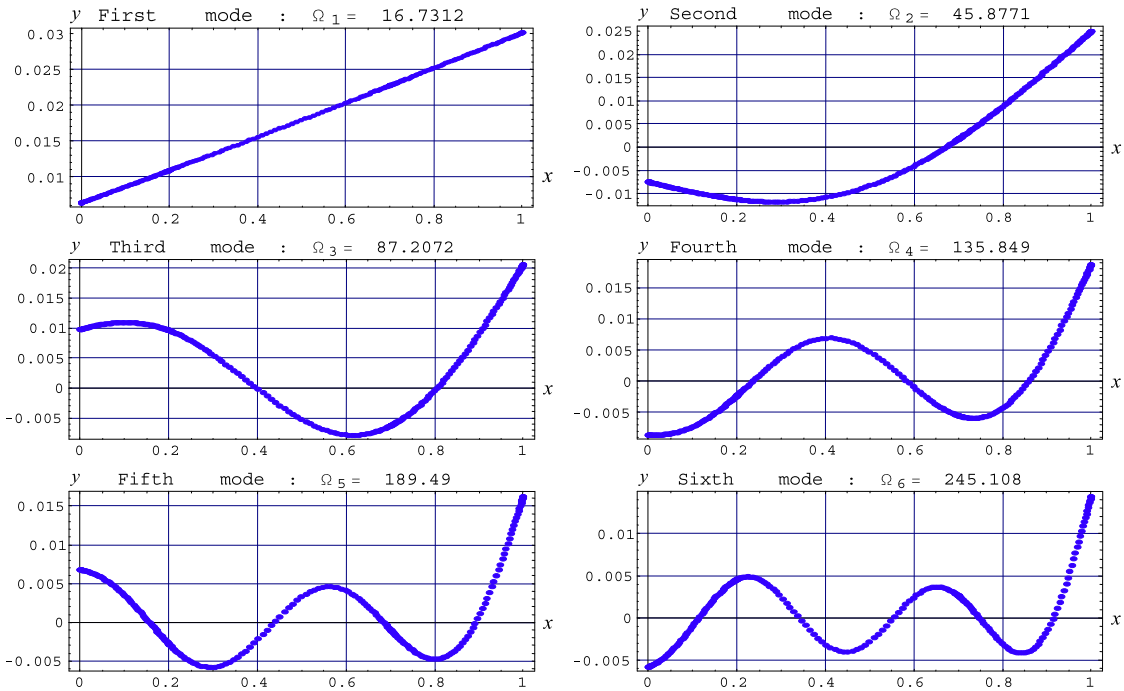

Fig. 10 The non-dimensional natural frequencies and mode shapes of a three span Timoshenko beam $R_1 = 0.5$; $s_1 = 30$; $K_{W1} = 1$; $K_{\psi 1} = 0.1$, $\eta = 15$

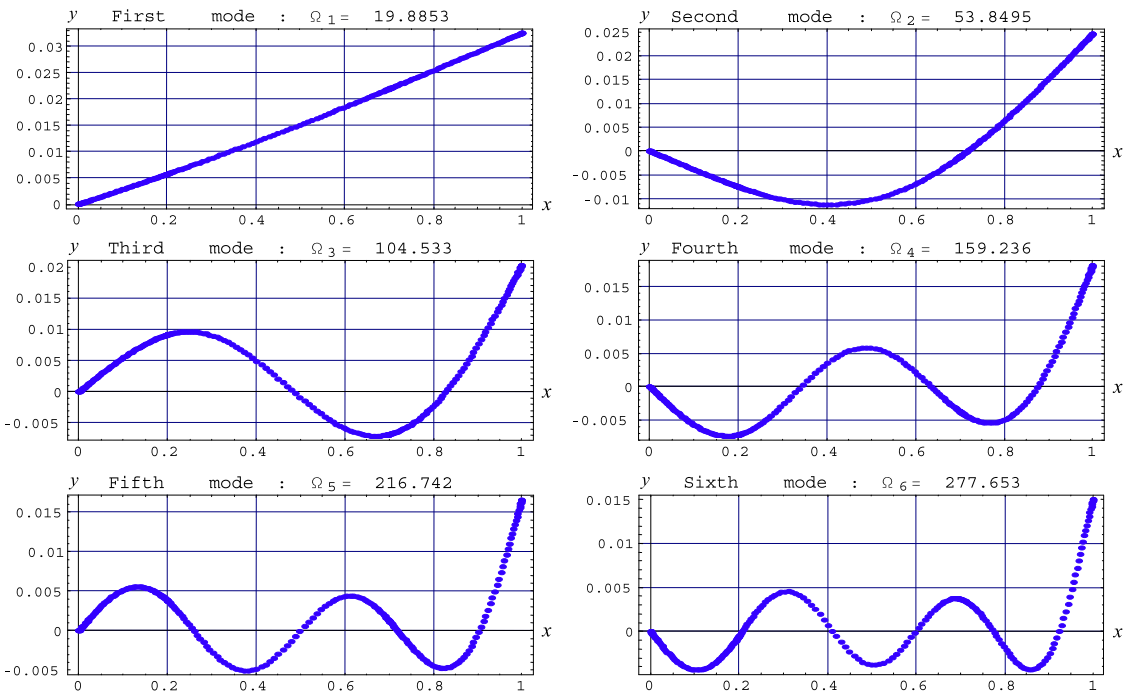

Fig. 11 The non-dimensional natural frequencies and mode shapes of a three span Timoshenko beam $R_1 = 0.5$; $s_1 = 30$; $K_{W1} = 1000000$; $K_{\psi 1} = 0.1$, $\eta = 15$

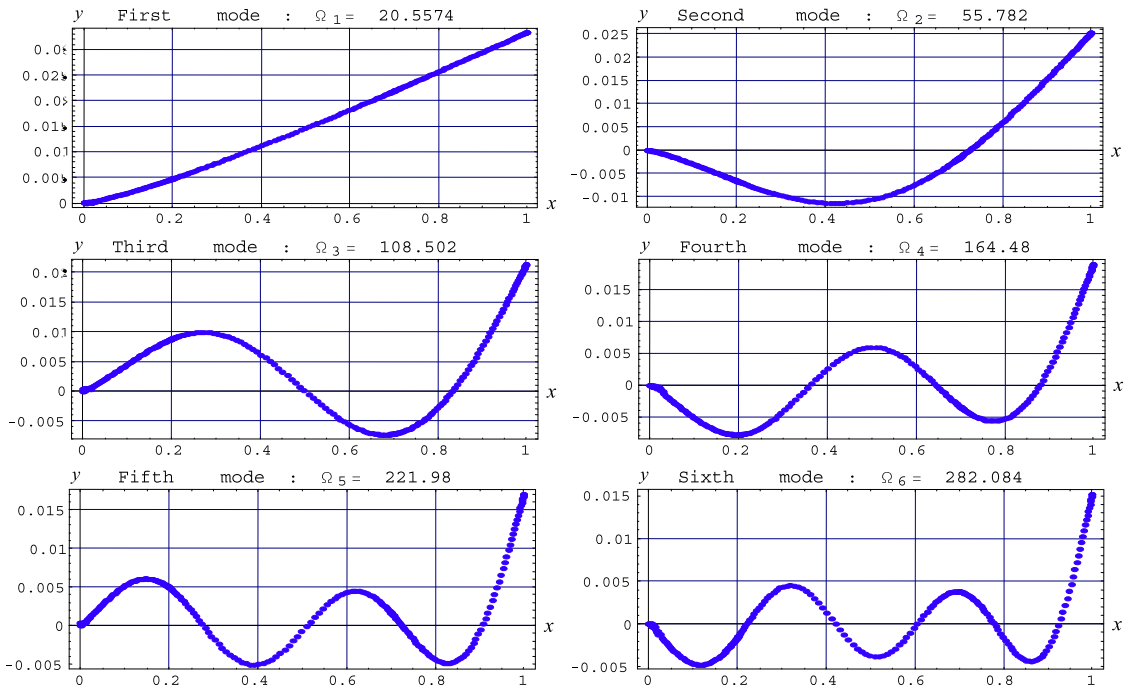

Fig. 12 The non-dimensional natural frequencies and mode shapes of a three span Timoshenko beam $R_1 = 0.5$; $s_1 = 30$; $K_{W1} = 1000000$; $K_{\psi 1} = 1000000$, $\eta = 15$

coefficient varies from 237.961 to 238.986 (0.43 %) (Table 9).

The last example corresponds to a three span beam with one step jump (Fig. 7). The beam characteristics are: $s_1 = 30$; $\nu = 0.30$; $\kappa = 0.849673$; $R_1 = 0.5$; $l_1 = 0.2$; $\alpha_1 = 1$; $c_{01} = 1$; $c_{11} = c_{21} = 0$; $l_2 = 0.5$; $\alpha_2 = 0.6667$; $c_{02} = 1$; $c_{12} = 2.5$; $c_{22} = -1.25$; $l_3 = 0.3$; $\alpha_3 = 1.5$; $c_{03} = 1$; $c_{13} = 0$; $c_{23} = -0.5778$. Figures 8 to 12 show the mode shapes and frequency coefficients for different relations of K_{W1} and $K_{\psi 1}$, at rotational speed $\eta = 15$.

The non-dimensional frequencies and mode shapes of the beam with $K_{W1} = 0.1$; $K_{\psi 1} = 0.01$ and the beam with $K_{W1} = 0.1$; $K_{\psi 1} = 1000000$ are very similar. There are slight differences in the corresponding frequency coefficients, less than 2.5 %, and the mode shapes are almost the same (Figs. 8 and 9).

In general, the effect of the rotational spring on the dynamic behavior of the rotating beam is small and in particular when $K_{W1} = 0.1$, it is negligible. Greater rigidity of the translational spring changes the mode shapes as shown in Figs. 8 to 12.

5 Conclusions

The convergence and accuracy of the present approach to analyze a rotating tapered multi-span beam have been validated by a detailed set of numerical examples, including the limiting case in which the cross section of the end of the beam tends to zero.

It can be concluded that the effect of the translational spring stiffness in the dynamic behavior of the rotating beam is much more pronounced than the effect of the rotational spring stiffness.

It is also observed that increasing the rotation speed has a greater influence on the lower frequency coefficients. This study shows that the model based on Timoshenko theory is particularly useful for determining the higher frequencies. In considering the practical implications of the proposed model, it is worth remembering that the process of raising the natural frequencies by removing appropriate mass of the original structure is generally defined as "dynamic stiffening", which is essentially a special chapter of the theory of optimization. Certainly a quadratic variation of the height of the cross section can be

used for modeling, by suitable determination of the constants of the polynomial, the attempt to optimize the natural frequencies of transverse vibration of the beam.

The differential quadrature method can be easily implemented by many optimization software codes, such as MATHEMATICA software [26].

Finally, the present analysis shows that an imperfection in the clamped condition will affect more the lower non-dimensional frequencies than the higher ones.

Acknowledgements The authors wish to express their gratitude to the Universidad Nacional del Sur and the Consejo Nacional de Investigaciones Científicas y Técnicas for the financial support which enable this work to be conducted.

References

1. Hodges DH, Rutkowoski MJ (1981) Free vibration analysis of rotating beams by a variable order finite element method. AIAA J 19:1459–1466
2. Naguleswaran S (2004) Transverse vibration of an uniform Euler–Bernoulli beam under linearly varying axial force. J Sound Vib 275:47–57
3. Banerjee JR (2000) Free vibration of centrifugally stiffened uniform and tapered beams using the dynamic stiffness method. J Sound Vib 233:857–875
4. Banerjee JR, Su H, Jackson DR (2006) Free vibration of rotating tapered beams using the dynamic stiffness method. J Sound Vib 298:1034–1054
5. Wang G, Wereley NM (2004) Free vibration analysis of rotating blades with uniform tapers. AIAA J 42(12):2429–2437
6. Özdemir Ö, Kaya MO (2006) Flapwise bending vibration analysis of double tapered rotating Euler–Bernoulli beam by using the differential transform method. Meccanica 41(6):661–670
7. Gunda JB, Ganguli R (2008) New rational interpolation functions for finite element analysis of rotating beams. Int J Mech Sci 50:578–588
8. Banerjee JR (2001) Dynamic stiffness formulation and free vibration analysis of centrifugally stiffened Timoshenko beams. J Sound Vib 247:97–115
9. Özdemir Ö, Kaya MO (2010) Vibration analysis of rotating tapered Timoshenko beam using DTM. Meccanica 45:33–42
10. Kumar A, Ganguli R (2009) Rotating beams and non rotating beams with shared eigenpair. J Appl Mech 76(5):1–14
11. Ganesh R, Ganguli R (2011) Physics based basis function for vibration analysis of high speed rotating beams. Struct Eng Mech 39:21–46
12. Attarnejad R, Shahba A (2011) Dynamic basic displacement functions in free vibration analysis of centrifugally stiffened tapered beams; a mechanical solution. Meccanica 46(6):1267–1281
13. Allahverdizadeh A, Mahjoob MJ, Eshraghi I, Asgharifard-S P (2012) Effects of electrorheological fluid core and functionally graded layers on the vibration behavior of a rotating composite beam. Meccanica 47(8):1945–1960
14. Laura PAA, Gutiérrez RH (1993) Analysis of vibrating Timoshenko beams using the differential quadrature method. Shock Vib 1:89–93
15. Bert CW, Malik M (1996) Differential quadrature method in computational mechanics. A review. Appl Mech Rev 49:1–27
16. Karami G, Malekzadeh P (2002) A new differential quadrature methodology for beam analysis and the associated DQEM. Comput Methods Appl Mech Eng 191:3509–3525
17. Karami G, Malekzadeh P, Shahpari SA (2003) A DQEM for vibration of shear deformable non-uniform beams with general boundary conditions. Eng Struct 25:1169–1178
18. Liu GR, Wu TY (2001) Vibration analysis of beams using the generalized differential quadrature rule and domain decomposition. J Sound Vib 246:461–481
19. Felix DH, Bambill DV, Rossi RE (2009) Análisis de vibración libre de una viga Timoshenko escalonada centrífugamente rigidizada mediante el método de quadratura diferencial. Rev Inte Mét Num Cálc Dis Ing 25:111–132
20. Bambill DV, Felix DH, Rossi RE (2010) Vibration analysis of rotating Timoshenko beams of means of the differential quadrature method. Struct Eng Mech 34(2):231–245
21. Bambill DV, Felix DH, Rossi RE, Ratazzi AR (2011) Free vibration analysis of centrifugally stiffened non uniform Timoshenko beams. In: Gokcek M (ed) Mechanical engineering, ISBN: 978-953-51-0505-3. Available from: http://www.intechopen.com/books/mechanical-engineering/free-vibration-analysis-of-centrifugally-stiffened-non-uniform-timoshenko-beams
22. Zong Z, Zhang YY (2009) Advanced differential quadrature methods. CRC Press, New York
23. Stephen NG (2002) On "A check on the accuracy of Timoshenko's beam theory". J Sound Vib 257(4):809–812
24. Rossi RE (2007) Introducción al análisis de vibraciones con el método de elementos finitos, ISBN: 978-987-1171-71-2. EdiUNS, Universidad Nacional del Sur, Bahía Blanca, Argentina
25. Weaver W, Timoshenko SP, Young DH (2011) Vibration problems in engineering. Oxford University Press, London
26. Wolfram S (2012) Mathematica 8